LIMNOLOGY
and
OCEANOGRAPHY

ASLO

Limnol. Oceanogr. 9999, 2020, 1–14

doi: 10.1002/lno.11627

Taxon-specific primary production rates on coral reefs in the Florida Keys

Daniel P. Owen,[1] Matthew H. Long ,[2] William K. Fitt,[3] Brian M. Hopkinson [1*]

[1]Department of Marine Sciences, University of Georgia, Athens, Georgia
[2]Marine Chemistry and Geochemistry Department, Woods Hole Oceanographic Institution, Falmouth, Massachusetts
[3]School of Ecology, University of Georgia, Athens, Georgia

Abstract

Coral reefs are known to have extremely high rates of primary production. However, common geochemical methods for determining bulk rates of reef metabolism cannot distinguish which organisms are responsible for primary production. Here we used a "bottom-up" approach to estimate the contribution of diverse primary producers including hard corals, octocorals, and algae to gross primary production on coral reefs by scaling up taxon-specific rates by the abundance of those taxa in the environment. Chamber-based production rates of the dominant primary producers were obtained as a function of irradiance, the primary short-term driver of photosynthesis. These rates were then combined with annotated three-dimensional (3D) reconstructions of reef sections and a simple light field model to estimate reef-scale gross and net primary production rates over time. At a degraded reef in the Florida Keys octocorals and algae were the main producers, but at a more intact site a scleractinian coral (*Acropora palmata*) was the most important producer. As a validation of the approach, rates of primary production estimated using the "bottom-up" approach were compared with in situ eddy covariance fluxes. The daily integrated rates agreed within 16%, though maximal production was ~ 35% lower in the "bottom-up" approach likely due to under-representation of octocorals and macroalgae in the 3D reconstructions. The "bottom up" approach yielded results that were largely consistent with the in situ measurements of primary production and irradiance with the significant benefit of providing taxon-specific and spatially-explicit primary production rates.

Coral reefs exhibit spectacular organismal diversity and have significant ecological, aesthetic and commercial value, especially in relation to fisheries and tourism (Hughes 1994; Bowen et al. 2013). Coral reefs are also some of the most productive ecosystems on earth with clear, warm, shallow waters promoting the proliferation of numerous aquatic primary producers (Gattuso et al. 1998; Long et al. 2013). The dominant primary producers on a coral reef include zooxanthellae (symbiotic photosynthetic dinoflagellates) found in scleractinian (hard) corals and octocorals, and a diverse array of benthic macro- and micro-algae. Scleractinian corals are the principal framework builders on coral reefs and are therefore the main contributor to the high level of surface habitat complexity within a reef ecosystem (Graham and Nash 2013). The complex three-dimensional (3D) structure of coral reefs combined with the high levels of productivity found within the system support a multitude of higher trophic organisms and provide ecosystem services that help support more than 275 million people world-wide (Burke et al. 2011). While it is clear that coral reefs are highly productive, the geochemical methods typically used to determine production provide little quantitative insight into which reef primary producers are responsible.

A better understanding of taxa-specific production patterns on coral reefs would provide insight into how energy and elements flow through coral reef food webs. On coral reefs, primary production by algal-symbionts is directly used by the coral hosts. Corals respire most of this material themselves (Muscatine et al. 1981; Edmunds and Davies 1986), and coral biomass is only grazed upon by a few specialist consumers such as crown-of-thorns starfish, specialist fish species, and *Drupella* snails (Moran 1986; Cole et al. 2008). While coral tissue is typically not heavily grazed, corals exude mucus and other dissolved organic matter (DOM) at high rates (up to 50% of the material translocated from algal-symbionts is excreted), most of which is consumed in the pelagic microbial loop (Crossland et al. 1980; Wild et al. 2004). In contrast to corals, algal primary production is directly consumed by numerous higher trophic level organisms. Algal turfs are highly productive and nearly all the production is consumed

*Correspondence: bmhopkin@uga.edu

Additional Supporting Information may be found in the online version of this article.

immediately by reef fishes and invertebrates (Hatcher and Larkum 1983; Carpenter 1986). Macroalgae are less abundant (at least on pristine reefs) than algal turfs, but when present are also grazed by diverse fish species (Choat et al. 2002; Bellwood et al. 2006). Though much algal production is grazed, DOM release from algae is also significant (Wild et al. 2010; Haas et al. 2011). In general, productivity by algal-symbionts supports the hosts, specialist consumers, and the microbial loop, while algal productivity supports diverse fish and invertebrate species.

The structure and health of coral reefs worldwide are increasingly and negatively impacted by natural and anthropogenic stressors. Coral reefs affected by decades of losses in reef herbivores due to overfishing, disease, excess of inputs of sediment and nutrients, thermally induced coral bleaching, damage from hurricanes, and other stresses are exhibiting community phase shifts from coral to algal and sponge dominance (Aronson and Precht 2001; Hughes et al. 2003; Pawlik and McMurray 2020). Coral reefs in some areas have documented hard coral cover decreases from 50% cover to 5% cover in a matter of years, with little signs of recovery for decades after (Hughes 1994; Gardner et al. 2003; Graham and Nash 2013). Further, in areas where the local herbivores are severely impacted, increases in macroalgae can produce massive amounts of labile organic matter that may increase the growth and activity of microbes that are pathogenic to corals (Barott and Rohwer 2012; Haas et al. 2016). These dynamics create a positive feedback loop that maintains algal dominance (Smith et al. 2006). Sponges have also increased in abundance on many reefs, especially in the Caribbean, claiming space once occupied by corals and potentially altering reef biogeochemistry (de Goeij et al. 2013; Pawlik and McMurray 2020). In many coral reef systems, these negative stressors have severely impacted the ecosystem processes and potentially the dynamics of ecosystem productivity. Being able to accurately partition production among reef community members will help us understand how reef community production is being affected by reef degradation, and in turn how these changes in production may affect energy flow and elemental cycling on reefs.

Development of new methods to measure coral reef ecosystem productivity has been ongoing for over half a century (e.g., Odum and Odum 1955). The two major approaches for determining reef-scale primary production are (1) geochemical approaches that use changes in chemical constituents (e.g., O_2, CO_2) as water flows over the reef to infer metabolic rates and (2) "bottom-up" approaches that integrate production rates of individual taxa using their abundance in the ecosystem to estimate community metabolic rates. Geochemical approaches include classic techniques such as "flow respirometry" (Gordon and Hamilton 1962) and more modern methods such as the boundary layer approach and eddy covariance, which couple temporal or spatial changes in O_2 with more sophisticated understandings of turbulent transport to infer metabolic rates (McGillis et al. 2011; Long et al. 2013; Takeshita et al. 2016). Geochemical approaches provide accurate, in situ production rates but are fundamentally limited to ecosystem-scale analysis ($\sim$ 10–1000 m^2 spatial resolution). In contrast, "bottom-up" approaches scale-up the production rates of individual taxa, typically obtained from metabolic chamber measurements in a lab, to ecosystem scale using the abundance of each taxa on the reef, commonly obtained from underwater transects (Naumann et al. 2013; Van Hoytema et al. 2016). "Bottom-up" approaches offer more information-rich views of reef-scale primary production, providing taxon-specific and spatially-explicit production rates, but have been infrequently applied.

Here, we develop and apply an improved "bottom-up" approach that makes use of new developments in computer vision and machine learning (e.g., Hopkinson et al. 2020) to more accurately map primary producers on reefs and includes a simple light-field model as light is the primary short-term control on production (Fig. 1). 3D reconstructions of coral reef sections are generated from video transects and automatically labeled to map the distribution (surface area) of primary producers on a reef. In parallel, chamber incubations of the dominant primary producers are used to determine taxon-specific primary production rates as a function of irradiance. These production rate functions are then applied to the primary producers in 3D reconstructions and combined with incident irradiances from a simple light field model to estimate primary production over time. The method provides an "information-

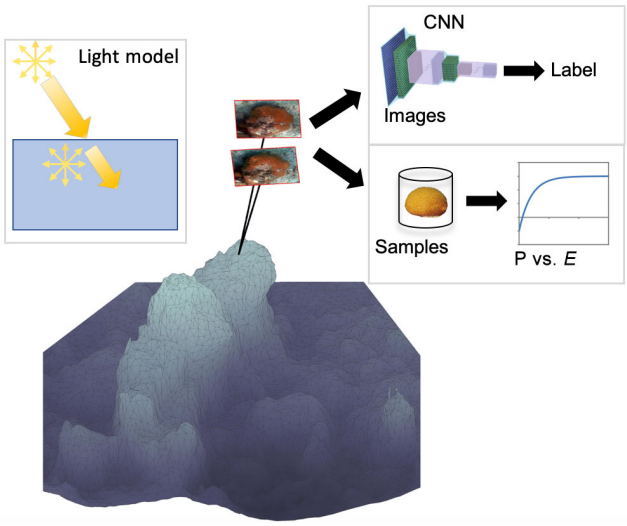

Fig. 1. Components of the "bottom up" reef productivity model. A 3D mesh reconstruction of the reef is created from images. The model estimates the productivity of each mesh element based on its identity, which is determined from images using a convolutional neural network (CNN), the productivity vs. irradiance of that taxa, determined from metabolic chamber incubations, and the light intensity on each mesh element, as estimated using a light field model that accounts for direct and diffuse irradiance.

rich" perspective on reef production, providing rates that are taxonomically, spatially, and temporally resolved.

Methods

Specimen collection and handling

Specimens were collected within Little Grecian Reef in the Northern Florida Keys (25.1185°N, 80.3005°W) under NOAA collection permits (FKNMS-2016-042, FKNMS-2016-082, FKNMS-2017-035). Collections were conducted in the summer over three consecutive years (June–July 2016, 2017, and 2018) and in winter over two consecutive years (December 2016 and 2017). Specimens of the dominant autotrophic taxa present at each reef site were taken during sampling. Specimens taken for metabolic study included the scleractinian corals *Orbicella annularis*, *Orbicella faveolata*, *Porites astreoides*, and *A. palmata*, octocorals within the genus *Antillogorgia*, *Gorgonia ventalina*, and various octocorals morphologically classified as "Sea Rods" (*Muricea* spp., *Eunicea* spp., *Plexaurella* spp., etc), the algal groups *Dictyota* spp., *Stypopodium* spp., *Halimeda* spp., and *Galaxaura* spp., as well as rubble with encrusting coralline algae and turf algae. All specimens were collected from different colonies to avoid pseudo-replication during metabolic measurements.

Specimens were immediately placed in seawater-filled Ziploc bags after removal and were transported back to the laboratory in seawater filled insulated coolers. Once on shore, specimens were labeled and placed in a recirculating holding tank filled with seawater collected from the reef sampling site. The temperature, salinity, and water level of the recirculating tank were monitored in order to keep the holding tank as close to the sampling environmental conditions as possible. A mesh screen was placed over the tank when it was in direct sunlight to keep irradiances below 600 μmol photons m^{-2} s^{-1} in order to avoid excessive heating and minimize stress. Samples were held upright or suspended from above to reduce stress and abrasion on the specimen. After collection, specimens were allowed to recover for at least 24 h before productivity measurements were taken, but were not held for more than 7 d.

Metabolic measurements

Photosynthesis (or respiration) as a function of irradiance (P vs. E) was determined through chamber incubations of the collected samples. The samples, depending on their physical size, were placed in either a 140 mL or 1200 mL clear acrylic, metabolic chamber in order to measure oxygen fluxes as a function of irradiance. The chambers were water-jacketed to maintain constant temperature and stirred with magnetic stir bars at rates that generate turbulent energy dissipation rates similar to in situ flow rates. Turbulent dissipation rates were estimated based on dye dispersion timescales in the chamber (Fischer et al. 1979). The freshly exposed portions of the scleractinian coral skeletons and rubble surfaces were covered with plasticine clay approximately 24 h prior to measurement to eliminate metabolic signals from internal cryptic organisms that would not naturally have been exposed. Oxygen concentrations were continuously recorded using a calibrated Firesting oxygen optode. Irradiance was then increased step-wise (0, 50, 100, 200, 300, 450, 900, and 0 μmol photons m^{-2} s^{-1}) holding light levels constant for 9 min at each irradiance. Light was delivered using computer-controlled LED light sources (Cool-White 5000K Cree) calibrated for each chamber via a Walz photosynthetically active radiation (PAR) meter. P vs. E data was fit to a saturating exponential function to extract the maximal gross photosynthetic rate (P_{max}), the light saturation parameter (E_k), and the dark respiration rate (R), which were subsequently normalized to specimen surface areas calculated as described below. Seawater blanks were measured for photosynthetic and respiratory activity periodically and maximal metabolic rates of the blanks were at least 10-fold lower than sample rates.

Specimen surface area calculations

Surface areas for the Scleractinia coral and rubble specimens were determined using the aluminum foil method (Marsh 1970). All other specimens were photographed against a gridded background, which was used to calibrate the images and correct for image angle orientation via a homography transformation (Hartley and Zisserman 2003). The outline of the macroalgal and octocoral samples (except for sea rods) in the corrected images were obtained in ImageJ, and the surface areas for each sample were calculated from the measured pixel area. In order to determine the surface area for sea rods samples, the radius and length of each branch was measured in ImageJ and surface area was calculated approximating each branch as a cylinder.

Annotated 3D reef site models

3D reconstructions of reef sections were created and automatically annotated as described in detail in Hopkinson et al. (2020). Briefly, stereo-video (2.7 k resolution at 30 frames s^{-1}, Dual GoPro 3 + Black) was acquired by swimming 1–3 m above the reef in a lawnmower pattern at sites on Little Grecian (25.1185°N, 80.3005°W) and Horseshoe (25.1393°N, 80.2945°W) reefs (Table 1). Images were extracted at 1–4 frames s^{-1} and 3D reconstructions were generated using Agisoft Photoscan and scaled using a custom approach. The 3D surface reconstructions (meshes) are composed of linked triangular elements (faces). The results of the 3D reconstructions have been described in detail in Hopkinson et al. 2020, in which the same reconstructions used here to assess primary production were used to test a method for automatic annotation. The 3D reconstructions show good general agreement with expected morphology and have few data gaps. They are composed of between $\sim$ 200,000 and 3 million linked triangular elements with sides averaging 1.6–4.6 cm, and total surface

Table 1. 3D reconstruction sites.

Site ID	Reef	Reef zone	Year/month	Post-hurricane
LG1	Little Grecian	Back reef	2015/7	No
LG2	Little Grecian	Back reef	2015/7	No
LG3	Little Grecian	Reef crest	2017/7	No
LG4	Little Grecian	Reef crest	2017/7	No
LG5	Little Grecian	Back reef	2017/12	Yes
LG6	Little Grecian	Back reef	2017/12	Yes
LG7	Little Grecian	Back reef	2017/12	Yes
LG8	Little Grecian	Back reef	2017/12	Yes
LG9	Little Grecian	Fore reef	2018/6	Yes
H1	Horseshoe	Reef crest	2015/7	No
H2	Horseshoe	Reef crest	2015/7	No

areas from 132 to 2349 m^2 (Table S1). Each specific site was only surveyed once at the time indicated in Table 1.

Each triangular mesh element was mapped back into the original images and a trained Convolutional Neural Network (CNN), nViewNet-8 (Hopkinson et al. 2020), was used to classify mesh elements into one of 13 categories. These 13 categories were defined as: Algae (macroalgae including *Dictyota* spp., *Stypopodium* spp., and *Halimeda* spp.), Galaxaura, Orbicella (*O. annularis* or *O. faveolata*), *P. astreoides*, *Siderastrea siderea*, *A. palmata*, *G. ventalina*, Antillogorgia, Sea Rods, Rubble, Sand, Other (visually identifiable sections of the reef benthos that are not any of the previous categories), and Unclassified (sections of reef benthos that could not be identified due to image quality) (Table 2). nViewNet-8 was trained on a manually annotated dataset of 15,804 points split into training (70%), validation (10%), and testing (20%) datasets. The overall classification accuracy on the testing dataset was 94.4% and most classes were classified with > 90% accuracy with the exception of *G. ventalina*, Sea Rods, Sand, and Unclassified (Fig. S1).

Table 2. Classes used in the convolutional neural network.

Class name	Description	*P* vs. *E* parameters
Algae	Macroalgae and/or dense turf algae	Average of all algae other than Galaxaura
Galaxaura	Galaxaura red macroalgae	Galaxaura
Antillogorgia	*Antillogorgia* spp. octocorals, commonly called sea plumes	Antillogorgia
G. ventalina	Sea fan *G. ventalina*	*G. ventalina*
Sea rods	A highly varied group of octocorals including Eunicea, Plexaura, Plexaurella, Muricea, etc	Sea rods
A. palmata	*A. palmata* coral	*A. palmata*
P. astreoides	*P. astreoides* coral	*P. astreoides*
S. siderea	*S. siderea* coral	Average of all corals
Orbicella	*O. faveolata* and *O. annularis* corals	Average of *O. faveolata* and *O. annularis*
Rubble	Bare coral rubble or rubble covered with crustose coralline algae or low density algal turf	Rubble
Sand	Loose sand	N/A
Other	Visually identifiable but not in the above categories	N/A
Unclassified	Poor image quality prevented identification	N/A

Light field model

A light field model was applied to the annotated 3D reef reconstructions in order to estimate the PAR intensity striking each mesh face over the course of a day. The model considers direct and diffuse PAR separately and then sums the intensities of these two components to calculate the total PAR irradiance incident on each mesh face. PAR (400–700 nm) is not spectrally resolved. The direct and diffuse irradiance at the ocean surface was determined using the Simplified Model of Atmospheric Radiative Transfer of Sunshine (SMARTS Windows version 2.9.5i1.3) (Gueymard 2005) using the subtropical reference atmosphere, maritime aerosol model, a regional and tilted surface albedo of water/calm ocean, and a spectral range of 400–700 nm, for the hours of 06 : 00–19 : 00 h on July 5 ("Summer") and 07 : 00–17 : 00 h on December 15 ("Winter") at Little Grecian Reef. For site LG9, the SMARTS "Summer" date was shifted to June 27 to align with eddy covariance productivity data collected at this location (see below). The model was run on surfaces at four evenly spaced tilt and azimuth angles to parameterize diffuse irradiance as a function of these angles.

As direct light passes through the air–water interface its intensity is reduced by reflection, which is treated using Fresnel's equation, and its angle is modified by refraction (Kirk 2011). The intensity of direct light is attenuated with distance traveled through the water based on a diffuse attenuation coefficient for downwelling irradiance (K_d) of 0.1 m^{-1} (based on Zepp et al. 2008 and Ong et al. 2018), accounting for light absorption and scattering by the water column above the reef benthos. When direct light intercepts a mesh element, the angle of incidence is used to determine the intensity and a ray is projected from mesh element back to the sun to ensure the line of sight is not blocked by another part of the mesh. The line of sight test is accelerated using a bounding volume hierarchy.

Diffuse PAR light is assumed to pass without loss through the air–water interface, but as it travels through the water it is attenuated based on a diffuse attenuation coefficient as described for direct irradiance. Diffuse light intensity striking a

mesh face has angular dependence and this dependence was accounted for using the orientation of the mesh face and interpolating between outputs of the SMARTS model at discrete tilt and azimuth angles. Direct and diffuse PAR irradiance incident on each face are then summed to determine the total PAR photosynthetic photon flux (μmol photons m^{-2} s^{-1}) on each mesh face over time, which is then used in the "bottom up" model.

Bottom-up model

The "bottom-up" model combines the annotated 3D reconstruction, light field model, and *P* vs. *E* relationships to estimate reef-scale production as illustrated in Fig. 1. The *P* vs. *E* parameters (P_{max}, E_k, *R*) for each taxa were averaged over all years and seasons (see "Results" section) and used to parameterize the reef-scale "bottom-up" production model (Table 2). The metabolic rates of *Dictyota* spp., *Stypopodium* spp., and *Halimeda* spp. were averaged together to apply to the "Algae" annotated surfaces. The metabolic rates of *O. annularis* and *O. faveolata* were averaged together to apply to the "*Orbicella*" annotated surfaces. The metabolic parameters for all scleractinian corals were averaged and applied to *S. siderea* annotated surfaces, since this species was not sampled. For all other taxa the measured metabolic rates were directly applied to the corresponding annotated surfaces though note that "Sea Rods" represent multiple genera. The Sand, Other, and Unclassified categories were assumed to have no significant photosynthetic activity compared to the other more dominant classes.

PAR intensities from the light field model were then used to calculate the photosynthetic rate of each mesh element over the course of the day. Production rates per mesh element were summed by taxa to determine taxon specific rates of production over time and integrated over the course of a day. These rates were then normalized by the planar area of the reef section. Gross primary production (GPP, neglecting autotroph respiration) and net primary production (NPP) were calculated in the summer and winter for all sites. NPP was only calculated over the daytime hours because all respiration rates were measured during the day, during which respiration rates are typically elevated over nighttime values ("light-enhanced respiration"; Kuhl et al. 1996, Langdon et al. 2003, Glud 2008) and so is referred to as "day-time integrated NPP."

The consequences of variability in *P* vs. *E* parameters and errors in class assignment by the CNN on outputs of the "bottom-up" model were assessed using a Monte-Carlo analysis since these sources of error are well constrained. *P* vs. *E* parameters (P_{max}, *R*, and E_k) for each taxa were perturbed from their mean values by draws from a standard Gaussian distribution scaled by the standard error of the mean for each parameter. Class assignments for each mesh element were flipped probabilistically based on assignment distributions from the confusion matrix (Fig. S1). The "bottom-up" model was then run on the perturbed inputs 100 times and variability in the model outputs (total production, fraction of total production by each taxa) was used to estimate errors. To assess the effects of errors in the light field model, the diffuse attenuation coefficient (K_d) was either doubled or reduced to half of its base value resulting in changes to both direct and diffuse irradiance. Source code for the bottom-up and light field models are publicly available (https://github.com/bmhopkinson/Bottom_up_model).

Eddy covariance measurements

An eddy covariance instrument was deployed at Little Grecian reef at the center of the area of the LG9 3D reconstruction for a period of 4 d (25 June 2018–29 June 2018) to determine the flux of oxygen across the reef-water interface. The system included an acoustic Doppler velocimeter (ADV, Nortek) coupled to a FirestingO_2 Mini fiber-optic O_2 meter with a temperature-compensated, fast-response (< 0.3 s), 430 μm diameter optode (Pyroscience, GE), as described in Long et al. (2019). The mean turbulent O_2 flux was calculated over 0.25 h periods from the product of the instantaneous variations in the vertical velocity and O_2 concentration by $F_{bw} = \overline{O_2' w'}$, where the prime values indicate the turbulent fluctuating components determined from Reynolds decomposition and the overbar indicates temporal averaging.

The system logged data from the ADV (3D velocity), O_2 optode, and an Inertial Measurement Unit (IMU) sensor at a frequency of 32 Hz. The height of the velocimeter measuring volume above the sediment surface was determined using relationships determined by Rheuban and Berg (2013) with measuring heights of 0.8 m over the high surface roughness environments of the reef (Long et al. 2013). The large measuring height and the presence of a biological canopy required the use of a storage correction to account for changes in the mean concentration (see Rheuban et al. 2014 and Long et al. 2015). A flow-through O_2 sensor design used a microfluidic volume and KNF micropump (model NF10, 100 mL min^{-1}) that was located 2.5 cm behind the measuring volume. All instruments were packaged onto a rotating base which allowed the precise correction for the separation between the sensors using the known sensor separation, current flow rate and the fact that that sensors were always oriented in line with the flow. The IMU measured the instrument orientation, movement and acceleration to allow for coordinate matrix transformation to account for platform rotation and movement (Long and Nicholson 2018) and is based on similar approaches used in atmospheric eddy covariance measurements (Edson et al. 1998, Flügge et al. 2016). The specific configurations, data treatment, and validation can be found in Long et al. (2019) and Long and Nicholson (2018). Additionally, in situ photosynthetically active radiation (PAR) was measured using a PAR logger (Odyssey, NZ) that was calibrated to a spherical quantum sensor (LICOR 193SA) by the methods of Long et al. (2012).

Statistical analyses

The statistical significance of differences in chamber-based metabolic rates between season and taxa was assessed using ANOVA analysis in *R*. The ability of taxonomic and structural variables to explain observed reef scale GPP rates were assessed using linear regression in *R*. For this analysis, there were 11 possible explanatory variables (10 different photosynthetic taxa and one structural variable, the ratio of total surface area to planar surface area) and only 11 observations resulting in a completely determined system of equations. Consequently, we first excluded low abundance taxa (*P. astreoides*, *S. siderea*, and Sea Rods) and then constructed a linear model with the remaining seven taxa and the index of structural complexity. This model was sequentially reduced by eliminating non-significant variables until a parsimonious model containing only significant variables was obtained.

Results

Metabolic measurements

A total of 211 samples of macroalgae, scleractinian corals, octocorals, and rubble were collected and subjected to photosynthesis vs. irradiance experiments over the course of 3 yr. The data from each sample was fit to a saturating exponential function to extract metabolic parameters (P_{max}, R, E_k). A two-way ANOVA assessing the significance of taxa and season on metabolic parameters indicated that taxa was a significant factor for all parameters whereas season (winter vs. summer) only significantly affected R. However, there was no significant interaction between season and taxa on R, and so all metabolic parameters were averaged across seasons.

The taxa were divided into three general groups based on P vs. E parameters: the first macroalgae, the second taxa with symbiotic, photosynthetic dinoflagellates (corals), and third Rubble, which hosts a complex mix of turf and crustose coralline alga (Fig. 2). P_{max} was similar across most taxa ($\sim 4 \times 10^{-4}$ μmol O_2 cm^{-2} s^{-1}) as indicated by overlap in the 95% confidence intervals of the mean (Fig. 2a). The macroalgae Galaxaura had notably high but variable P_{max} ($\sim 7 \times 10^{-4}$ μmol O_2 cm^{-2} s^{-1}) and Sea Rods and Rubble had significantly lower P_{max} than most other taxa ($\sim 1.5 \times 10^{-4}$ μmol O_2 cm^{-2} s^{-1}). R was generally low and similar among the macroalgae ($\sim -1 \times 10^{-4}$ μmol O_2 cm^{-2} s^{-1}, the negative value indicating consumption of O_2) but was typically higher in the coral group ($\sim -2 \times 10^{-4}$ μmol O_2 cm^{-2} s^{-1}) with the notable exception of Sea Rods (Fig. 2b). Rubble had low respiration rates similar to Sea Rods ($\sim -0.5 \times 10^{-4}$ μmol O_2 cm^{-2} s^{-1}). The light saturation constant (E_k) was similar among nearly all taxa (~ 150 μmol photons m^{-2} s^{-1}) except Rubble, which had a statistically significantly higher E_k (~ 250 μmol photons m^{-2} s^{-1}, Fig. 2c). E_k for *A. palmata* was highly variable in part due to the small sample size ($n = 3$).

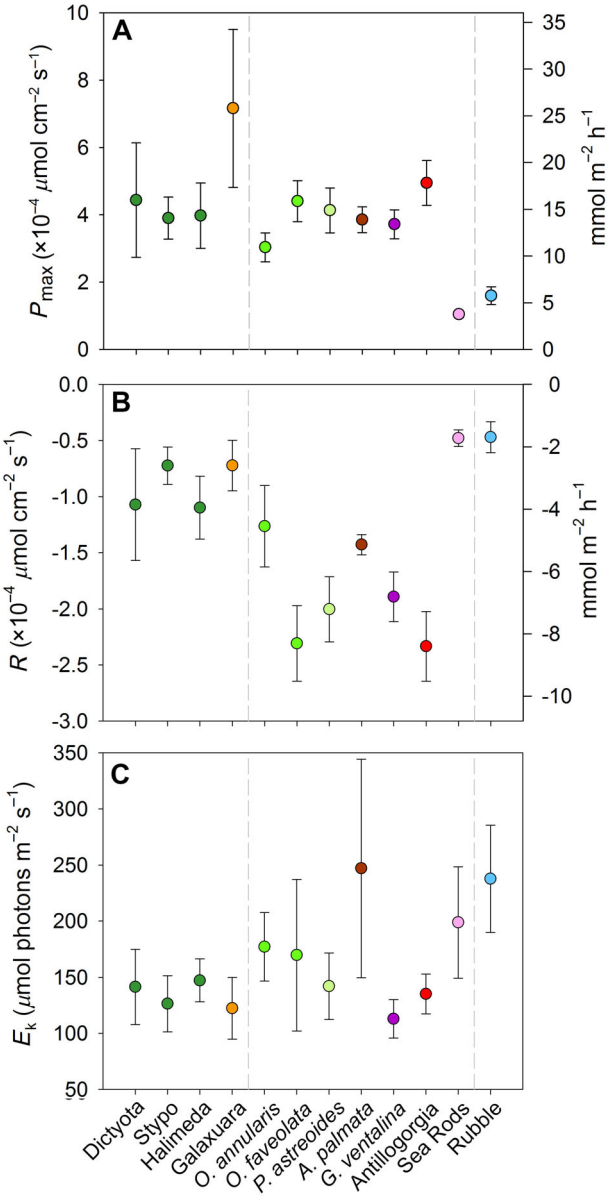

Fig. 2. Results of chamber metabolic measurements on reef primary producers. **(a)** Maximal photosynthetic rates (P_{max}), **(b)** respiration rates (R), and **(c)** the light saturation parameter (E_k). The dashed vertical lines separate three major groups: macroalgae (left), coral and octocorals (center), and rubble (left) which is partially covered with turf and crustose coralline algae. Points are mean values and error bars indicate 95% confidence intervals.

3D reef scale primary production

The "Bottom-up" approach was used to determine taxonomically, spatially, and temporally resolved GPP and NPP on 11 different reef sections using summer and winter light fields. A typical result is shown in Fig. 3 illustrating that GPP and NPP rise rapidly in the morning since light intensities quickly exceed E_k for most taxa soon after sunrise (Fig. S2), remain roughly constant throughout most of the day, and then decline rapidly just before sunset as irradiance drops below E_k.

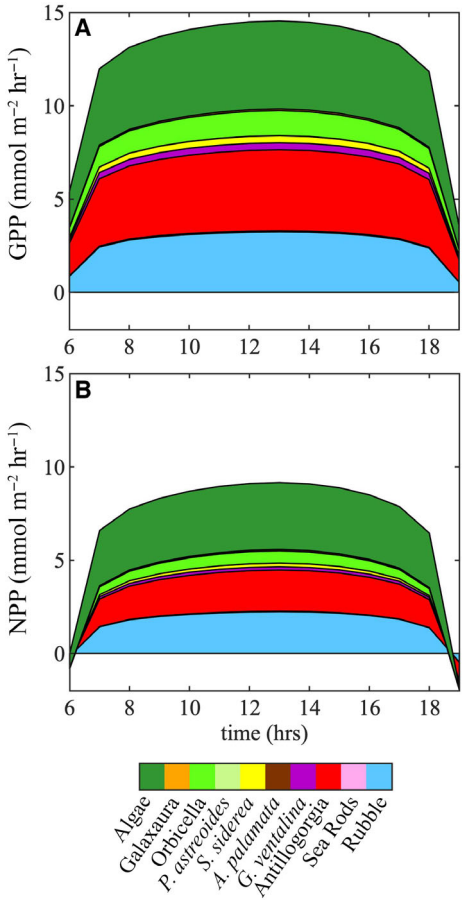

Fig. 3. Sample results of **(a)** taxon-resolved GPP and **(b)** day-time integrated NPP vs. time from site LG2.

Daily integrated GPP ranged from 127 to 258 mmol O_2 m^{-2} d^{-1} (average: 198 ± 36) in the summer and from 90 to 188 mmol O_2 m^{-2} d^{-1} (average: 141 ± 26) in the winter (Fig. 4). Day-time integrated NPP ranged from 75 to 205 mmol O_2 m^{-2} d^{-1} (average: 123 ± 41) in the summer and from 50 to 145 mmol O_2 m^{-2} d^{-1} (average: 83 ± 31) in the winter. NPP was 39% ± 11% lower (average and SD among sites) than GPP in summer and 43% ± 11% lower than GPP in winter. GPP decreased by 28% ± 1% and NPP decreased by 33% ± 3% from summer to winter primarily due to a reduced number of daylight hours. However, potential seasonal changes in benthic cover, especially macroalgae (Lirman and Biber 2000; Duran et al. 2016), were not incorporated into these estimates since the same 3D constructions (captured in a single season) were used in both summer and winter production simulations.

In a given season, the taxonomic composition of the primary producers exerts primary control on reef-scale GPP and NPP based on multiple linear regression analyses (Table 3). Just two variables (the fraction of surface area covered by Galaxaura and Rubble) were able to explain ≧98% of the variance in GPP and NPP, and only in one case (NPP in winter) was structural complexity a significant explanatory variable.

On Little Grecian reef production was primarily from Algae, Rubble, and octocorals (*G. ventalina* and Antillogorgia) with Galaxaura algae important on sites sampled after Hurricane Irma in September 2017 (LG5-LG9, Fig. 4). In contrast, production on Horseshoe Reef was dominated by *A. palmata* and Rubble. The relative contribution of each taxon to total GPP was roughly proportional to its contribution to total productive surface area (the combined surface area of all photosynthetic taxa), with Galaxaura notably over-contributing to productivity and Rubble under-contributing (Fig. 5).

A Monte Carlo error analysis showed that uncertainties in *P* vs. *E* parameters and errors in mesh labeling by the CNN had relatively small effects on inferred total GPP, NPP, and the proportions of productivity contributed by different taxa (Tables S2, S3). Absolute SD of GPP ranged from 4.9 to 30.2 mmol O_2 m^{-2} d^{-1}, averaging 11.8 mmol O_2 m^{-2} d^{-1} over the 11 sites sampled. Relative SD (100 × SD/mean) in summer GPP ranged from 2.9% to 11.8% and averaged 5.7%. Absolute SD of NPP ranged from 5.6 to 28.3 mmol O_2 m^{-2} d^{-1}, averaging 12.1 mmol O_2 m^{-2} d^{-1} over the 11 sites sampled and relative SD ranged from 6.6% to 14.0% and averaged 9.2%. Absolute errors in the percent contribution of different taxa to GPP ranged from 0% to 4.4% and averaged 0.7%, but note that many of the percent contributions are zero or near zero. Relative SD in the contribution of different taxa to GPP ranged from 0% to 22.2% and averaged 7.2%. Absolute SD in the percent contribution of different taxa to NPP ranged from 0% to 5.2% and averaged 1.2%, while relative SD ranged from 0% to 33.3% and averaged 14.7%.

The quality of the light field model was compared to diel in situ PAR measurements at one site where these measurements were available (LG9). Comparison of the modeled PAR values with PAR data showed good agreement between the model and data in the morning, underestimation by the model in the middle of the day, and slight overestimation by the model toward the end of the day (Fig. S3). Underestimation in the middle of the day is likely due to neglect of benthic light scattering in the model, which can be significant in carbonate systems (Joyce and Phinn 2002; Dierssen et al. 2009). To assess the potential effect of errors in the modeled light field on inferred production a sensitivity analysis was conducted in which light intensity was varied by modifying K_d, the diffuse attenuation coefficient. This assessment showed that total production was only slightly sensitive to variations in light intensity with production changing by ~ 3% for a 10% variation (increase or decrease) in average irradiance (Table S4), in large part because primary producers are saturated for light for most of the day (Figs. S2, S4).

Eddy covariance

In situ oxygen fluxes were determined with the eddy covariance instrument continuously over a 4 d period at site LG9 (Fig. S5). Fluxes range from ~ 20 mmol O_2 m^{-2} h^{-1} during the daytime to –50 mmol O_2 m^{-2} h^{-1} during the night. The NCP rates were largely negative over the entire 4 d

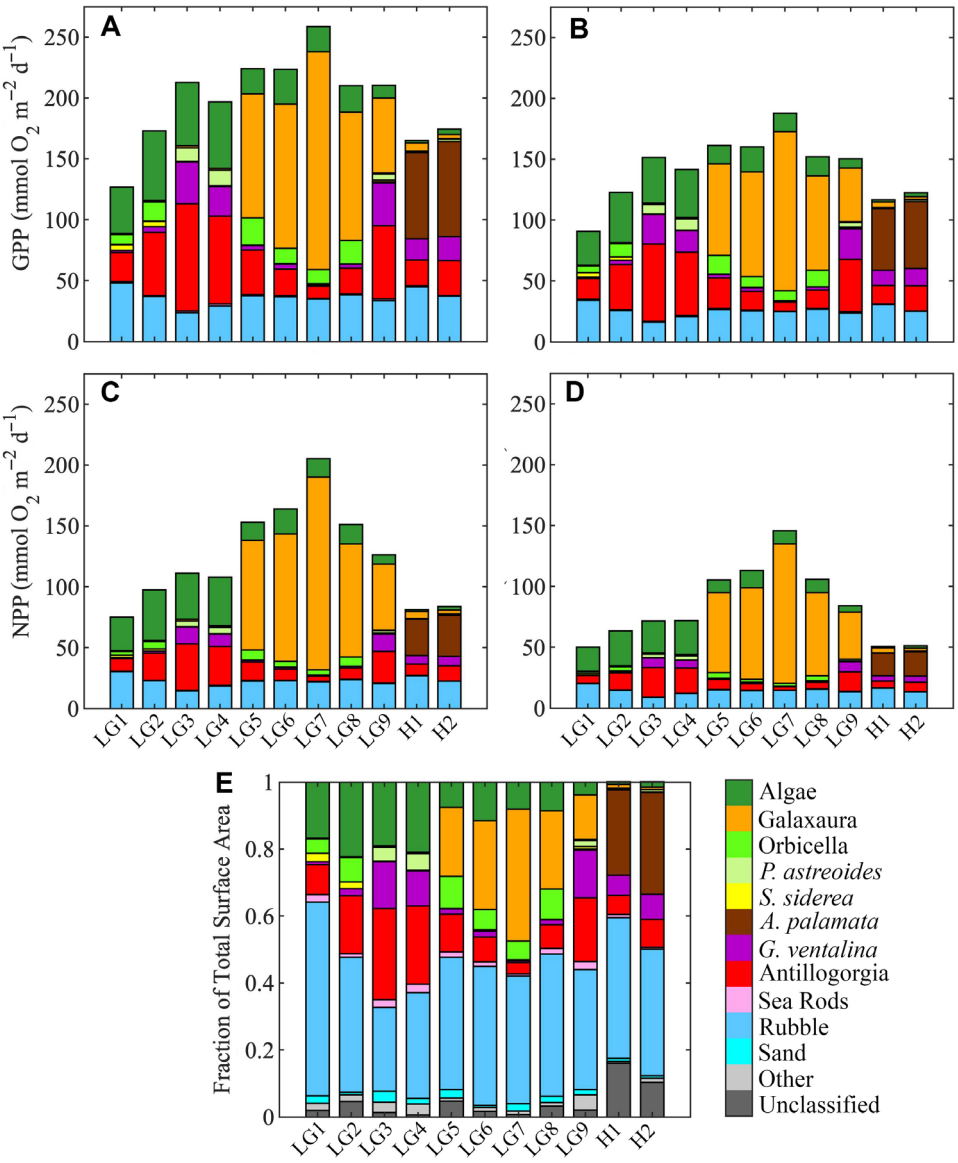

Fig. 4. Daily integrated (**a**) summer GPP, **(b)** winter GPP, **(c)** summer day-time integrated NPP, and **(d)** winter day-time integrated NPP. Panel **(e)** shows the fraction of surface area in each class by site.

deployment except during brief periods during the afternoon. To compare the bottom up GPP estimate to the eddy covariance fluxes, hourly rates of GPP were estimated from the eddy covariance data by subtracting interpolated respiration rates (Fig. 6). The daytime respiration rates were linearly interpolated across the daytime period (e.g., hour 6–19) from the early morning respiration rates (e.g., hour 0–6) and the late night respiration rates (i.e., hour 19–23). The mean (n = 4 d) integrated GPP was 251.0 mmol O_2 m^{-2} d^{-1} was similar to the mean GPP predicted by the bottom up approach at this site, 210.5 mmol O_2 m^{-2} d^{-1}, representing a difference of only 16.2% between the two methods, but maximum GPP rates ($\sim$ 27 mmol O_2 m^{-2} h^{-1}) exceeded those of the bottom-up approach ($\sim$ 17.5 mmol O_2 m^{-2} h^{-1}) by 35.2%.

Discussion

Coral reefs are known to be one of the most highly productive marine ecosystems and they support a closely associated, diverse invertebrate and fish community (Gattuso et al. 1998; Bellwood et al. 2017). Techniques commonly used to determine reef productivity (flow respirometry, eddy covariance, boundary layer approach) are based on changes in oxygen concentrations in waters overlying the reef and are not

Table 3. Linear regression analysis of factors explaining GPP and day-time integrated NPP. GPP and NPP in each season were regressed against the fraction of surface area (SA) of Galaxaura and Rubble, and an index of 3D structural complexity, the ratio of total SA to planar SA (Table S1). For each explanatory variable the *p*-value in the multiple linear regression is reported. The R^2 value for the model using only the statistically significant explanatory variables is reported in the final column.

Rate/ season	SA galax	SA rubble	Total SA/planar SA	R^2
GPP/summer	<0.001	<0.001	0.053	0.99
GPP/winter	<0.001	<0.001	0.21	0.99
NPP/summer	<0.001	<0.001	0.064	0.98
NPP/winter	<0.001	<0.001	0.023	0.99

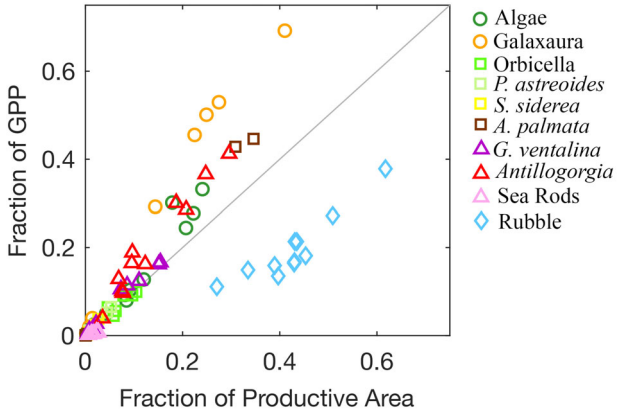

Fig. 5. Contribution of taxa to GPP vs. contribution to productive surface area from all sites. The solid line indicates a 1 : 1 relationship.

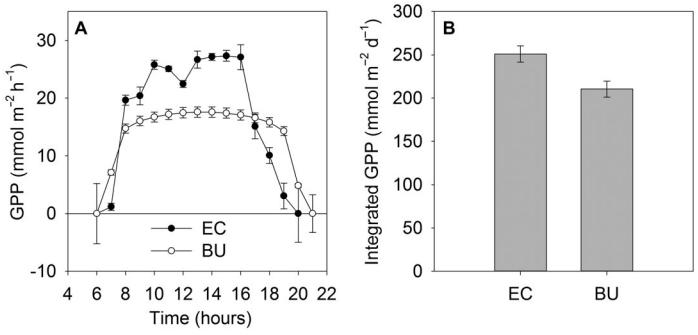

Fig. 6. Comparison of Eddy covariance-based GPP (EC) with "bottom-up"-based GPP (BU) at LG9 **(a)** over a diel cycle and **(b)** integrated over a day.

capable of resolving the taxa responsible for production. There have been a few attempts to determine the contributions of different taxa to total productivity in reefs and associated systems (Naumann et al. 2013; Van Hoytema et al. 2016). In these "bottom-up" approaches chamber-based production rates of corals, algae, and other components of the community were made and scaled up to the entire reef based on their percent cover (percent of occupancy when viewed from overhead), using a 2D–3D correction factor to account for the disparity between the 2D percent cover estimate and the 3D nature of the reef. Here an improved version of such an approach was taken using 3D surface reconstructions of reef sections to directly capture the 3D structure of the reef and accounting for the light dependence of production, since light is the primary short-term driver of production on coral reefs (Long et al. 2013). This approach was enabled by advances in computer vision (Hartley and Zisserman 2003) and machine learning (LeCun et al. 2015) that make it possible to generate and automatically label 3D surface reconstructions of reefs from images (Hopkinson et al. 2020).

This new "bottom-up" approach was employed at 11 sites on two reefs in the Florida Keys sampled over the course of 3 yr. As measured by this new approach, productivity (GPP and NPP) rose quickly in the early morning hours and remained at maximal rates for most of the day, declining only in the late evening hours (Fig. 3). Total PAR intensities on most surfaces exceeded E_k ($\sim$ 150 μmol photons m^{-2} s^{-1}) early in the morning meaning that production was light saturated throughout most of the day (Fig. S2). Diffuse light was an especially important component of this as it illuminated surfaces that were oriented away from direct sunlight. The effect of errors in *P* vs. *E* parameters and mesh labeling via a CNN were assessed using a Monte Carlo analysis, which showed that these sources of error had relatively modest effects on total production and the fraction of production contributed by different taxa (Tables S2, S3). Because light intensities greatly exceeded E_k on most surfaces for most of the day, the productivity results were not very sensitive to parameterization of the light model. Total production varied by $\sim$ 3% for a 10% change in average irradiance, and the relative contributions of taxa to total production was effectively invariant to changes in irradiance (Table S4). While the reefs studied here are very shallow (1–3 m deep) and well-illuminated, application of this approach to deeper reefs may require more careful parameterization and design of the light-field model.

Comparison of reef scale production rates determined using the "bottom-up" method with a geochemical technique at one site (LG9) indicates that the "bottom-up" method performs reasonably well (Fig. 6), with daily integrated GPP rates (210 mmol m^{-2} d^{-1}) that were within 16% of the in situ eddy covariance rate (251 mmol m^{-2} d^{-1}). While the integrated rates were similar, the "bottom-up" approach appears to underestimate maximal GPP. Reef scale maximal photosynthetic rates estimated by the "bottom-up" method were up to 17.5 mmol O_2 m^{-2} h^{-1} at site LG9, whereas eddy covariance rates ($\sim$ 27 mmol O_2 m^{-2} h^{-1}) were moderately higher. Multiple sources of error including errors in the light field model, differences between in situ and chamber production, and

incomplete representation of photosynthetic surface area in the 3D reconstructions potentially account for this discrepancy. The light field model underestimated midday irradiances (Fig. S3) but this error can only account for a small portion of the discrepancy between eddy-covariance and "bottom-up" maximal production because primary producers were already approximately light saturated (Figs. S2, S4). When the "bottom-up" model was forced with the observed PAR intensities maximal photosynthetic rates increase only ~ 5% (to 18.4 mmol O_2 m^{-2} h^{-1}). It is possible that collection and maintenance of specimens for laboratory P vs. E measurements stressed the organisms, reducing maximal photosynthetic rates, despite care taken to minimize these effects. If this is an issue, it appears to be a systematic consequence of ex situ measurement since the production rates we measured are very similar to those measured by other investigators (see a compilation in table S1 of Sawall and Hochberg 2018). An additional source of potential bias is that the 3D reconstructions only capture the surface of organisms at a resolution of ~ 3 cm. While this accurately represents some primary producers such as corals and the turf and crustose coralline algae that cover rubble, it does not fully capture producers such as macroalgae and octocorals that have branching morphologies and form volumetric assemblages. The 3D reconstructions only capture the outer surface of these assemblages. Additional sources of bias may include the natural in situ variability of drivers that are not captured in ex situ incubations (currents, nutrients, diel variability, etc.) and uncertainties in determining the contributing area or "footprint" of the eddy covariance technique. Furthermore, EC-based GPP rates likely underestimate true GPP because nighttime respiration rates, which are typically lower than daytime rates due to light-enhanced respiration (Kuhl et al. 1996, Langdon et al. 2003, Glud 2008), were used to convert observed NCP to GPP. While these methodological differences and biases are expected, the general agreement of the integrated rates suggests that both methods are suitable for determining reef GPP and both provide different insights into reef metabolism.

While geochemical approaches may ultimately provide more accurate estimates of total production, the main purpose of the "bottom-up" approach is to provide taxonomically-resolved rates of primary production (Figs. 3, 4). This information is important for understanding how carbon and energy flow through coral reef food webs and how these flows may change as the community composition of reefs is altered due to reef degradation (Carpenter 1986; Haas et al. 2016). At all sites, the turf and crustose coralline algae covering coral rubble provided a consistent base of production (at ~ 35 mmol O_2 m^{-2} d^{-1} GPP in summer) comprising ~ 20% of total GPP and NPP. Taxa responsible for the remaining production varied substantially between reefs and over time (Fig. 4). On Little Grecian reef, a highly degraded reef with low coral cover typical of the Florida Keys, production at sites sampled in summer 2015 and summer 2017 (LG1–LG4) was primarily contributed by the octocorals Antillogorgia and *G. ventalina* (~ 40%) and Algae (~ 30%). At sites sampled after passage of Hurricane Irma in September 2017 (LG5–LG9), Galaxaura, a red alga, proliferated dominating production on most sites (~ 50%), with smaller contributions from octocorals (~ 20%), illustrating that sources of production can change rapidly with environmental forcings. On Horseshoe Reef (H1–H2), an atypical reef still containing large stands of *A. palmata*, which used to dominate shallow reefs in Florida prior to degradation (Aronson and Precht 2001), production from *A. palmata* was substantial (~ 40% of GPP and NPP) with contributions from octocorals (~ 25%) but almost no macroalgae production (~ 3%). The Horseshoe sites were only sampled before Hurricane Irma, so it is unclear what impact this hurricane had on Horseshoe's productivity. On a relatively pristine reef with high coral cover in the Red Sea van Hoytema et al. (2016) found that hard corals were responsible for > 50% of GPP with soft corals a secondary factor and algae of all types contributing only ~ 20% to GPP. These results demonstrate, perhaps not surprisingly, that reef degradation shifts production, as well as abundance (Hughes et al. 2007; Ruzicka et al. 2013), from hard corals toward soft corals and algae. As discussed above, it is likely that productivity from clumped producers such as macroalgae and Antillogorgia are underestimated. Consequently, the shift from hard coral and turf/crustose coralline algae production to macroalgae and octocoral production with reef degradation are likely to be even more dramatic than estimated here.

The effects of reef degradation on total production will depend on both changes in the taxonomic composition of primary producers and reef structural complexity. At the 11 sites surveyed here taxonomic composition was the major determinant of total system production (Table 3) and these differences could be explained almost entirely by the amount of Rubble, with low productivity, or Galaxaura, a highly productive red alga. While this may suggest production will increase as macroalgae take over degraded reefs, Galaxaura appears to be an anomaly as the GPP rates of most algal species per unit surface area were similar to those of hard corals (Figs. 2, 5). This suggests that the total surface area of producers is likely to be a major control on reef-scale production in many cases. On the one hand, the loss of hard corals during the course of degradation ultimately leads to lowered structural complexity as the coral skeletons that form most of the reef's 3D structure break down (Alvarez-Filip et al. 2009; Graham and Nash 2013), suggesting total productive surface area may decrease. However, the macroalgae and octocorals that replace hard corals often have complex morphologies with high total surface area and so the overall effect of reef degradation on reef-scale production may be more complicated.

Although the degraded reefs studied here have high GPP, as indicated by both the "bottom up" and EC methods, EC-based NCP rates at LG9 showed that the system was net

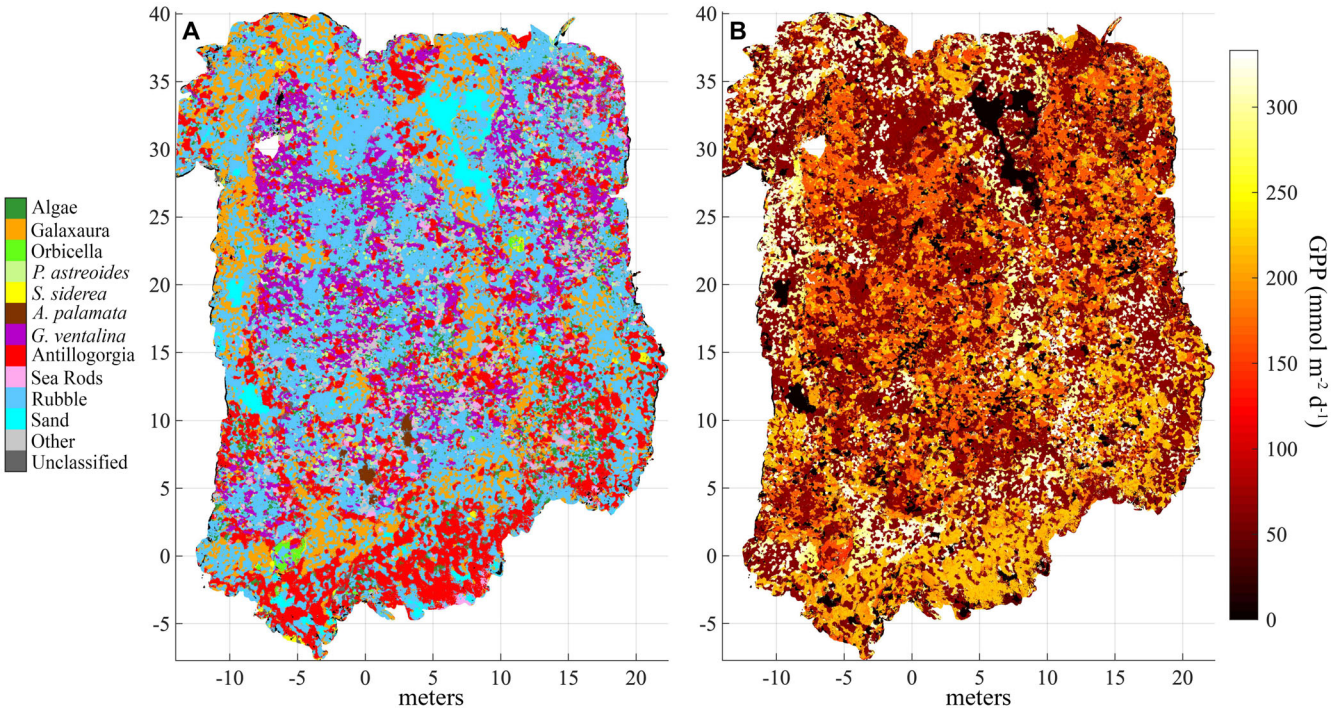

Fig. 7. Maps of **(a)** reef organisms and substrates and **(b)** daily integrated primary production at site LG9.

heterotrophic even during mid-day (Fig. S5) when most coral reefs have positive NCP (McGillis et al. 2011; Long et al. 2013; Takeshita et al. 2016). Potential explanations for net heterotrophy at this site include taxonomic differences from typical coral reefs, most notably a lower abundance of hard corals, or longer-timescale temporal decoupling (e.g., seasonal) between production and respiration, but we suspect the most likely explanation is high respiration rates from organisms within the reef framework (Richter et al. 2001). Most relevant to the work at hand, this observation highlights the inability of the "bottom-up" method to capture the often substantial respiration of heterotrophic cryptic and endolithic communities throughout the reef framework (Richter et al. 2001; Mueller et al. 2014), since the "bottom-up" method only incorporates the surficial community observable via photography.

Although we focus here on the "bottom-up" method's ability to produce taxon-specific production rates, it is also capable of generating spatially explicit estimates of production over the reef as shown in Fig. 7. Notable features include the high productivity associated with bands of Galaxaura around the edge of the reef section (low stands) and lower rates of production associated with rubble. These spatially explicit fluxes could provide insight into hotspots of food availability for fauna or be integrated into physical ocean models to better understand oxygen or carbon fluxes on the reef and exchanges with the adjacent ocean. Furthermore, the "bottom-up" approach is not limited to estimating production rates. The approach could be adapted to estimate reef-scale fluxes of dissolved organic carbon (Haas et al. 2016), nitrogen, or even sponge mediated transformations (Pawlik and McMurray 2020).

Conclusions

Using an improved "bottom-up" method, taxon specific rates of production on coral reefs in the Florida Keys were assessed. At all sites, turf algae and crustose coralline algae growing on coral rubble provided a consistent base of production (~ 20% of total), supporting fish and invertebrates (Carpenter 1986). On a more pristine reef, hard corals and octocorals were responsible for most of the production and macroalgal production was extremely low, consistent with previous observations in the Red Sea (Van Hoytema et al. 2016). However, on degraded reefs macroalgae and octocorals dominated production, potentially inhibiting reef recovery through release of dissolved organic matter that promotes growth of harmful microbes (Barott and Rohwer 2012). A highly productive red algae, Galaxaura, grew rapidly after the passage of a hurricane shifting the dominant sources of production on the reef. Comparison of the "bottom-up" approach with eddy covariance measurements showed the "bottom-up" method was reasonably accurate with daily integrated and maximal production estimates from the "bottom-up" method being somewhat lower. Nonetheless, this comparison shows the "bottom-up" approach is capturing the bulk of reef production and can be used to provide taxonomically, spatially, and temporally resolved production rates.

References

Alvarez-Filip, L., N. K. Dulvy, J. A. Gill, I. M. Cote, and A. R. Watkinson. 2009. Flattening of Caribbean coral reefs: Region-wide declines in architectural complexity. Proc. R. Soc. B-Biol. Sci. **276**: 3019–3025. https://doi.org/10.1098/rspb.2009.0339

Aronson, R. B., and W. F. Precht. 2001. White-band disease and the changing face of Caribbean coral reefs. Hydrobiologia **460**: 25–38. https://doi.org/10.1023/A:1013103928980

Barott, K. L., and F. L. Rohwer. 2012. Unseen players shape benthic competition on coral reefs. Trends Microbiol. **20**: 621–628. https://doi.org/10.1016/j.tim.2012.08.004

Bellwood, D. R., T. P. Hughes, and A. S. Hoey. 2006. Sleeping functional group drives coral-reef recovery. Curr. Biol. **16**: 2434–2439. https://doi.org/10.1016/j.cub.2006.10.030

Bellwood, D. R., C. H. R. Goatley, and O. Bellwood. 2017. The evolution of fishes and corals on reefs: Form, function and interdependence. Biol. Rev. **92**: 878–901. https://doi.org/10.1111/brv.12259

Bowen, B. W., L. A. Rocha, R. J. Toonen, S. A. Karl, and L. Tobo. 2013. The origins of tropical marine biodiversity. Trends Ecol. Evol. **28**: 359–366. https://doi.org/10.1016/j.tree.2013.01.018

Burke, L., K. Reytar, M. Spalding, and A. Perry. 2011. Reefs at risk revisited. World Resources Institute.

Carpenter, R. C. 1986. Partitioning herbivory and its effects on coral-reef algal communities. Ecol. Monogr. **56**: 345–363. https://doi.org/10.2307/1942551

Choat, J. H., K. D. Clements, and W. D. Robbins. 2002. The trophic status of herbivorous fishes on coral reefs - I: Dietary analyses. Mar. Biol. **140**: 613–623. https://doi.org/10.1007/s00227-001-0715-3

Cole, A. J., M. S. Pratchett, and G. P. Jones. 2008. Diversity and functional importance of coral-feeding fishes on tropical coral reefs. Fish Fish. **9**: 286–307. https://doi.org/10.1111/j.1467-2979.2008.00290.x

Crossland, C. J., D. J. Barnes, and M. A. Borowitzka. 1980. Diurnal lipid and mucus production in the staghorn coral *Acropora acuminata*. Mar. Biol. **60**: 81–90. https://doi.org/10.1007/BF00389151

de Goeij, J. M., D. van Oevelen, M. J. A. Vermeij, R. Osinga, J. J. Middelburg, A. F. P. M. de Goeij, and W. Admiraal. 2013. Surving in a marine desert: The sponge loop retains resources within coral reefs. Science **342**: 108–110. https://doi.org/10.1126/science.1241981

Dierssen, H. M., R. C. Zimmerman, and D. J. Burdige. 2009. Optics and remote sensing of Bahamian carbonate sediment whitings and potential relationship to wind-driven Langmuir circulation. Biogeosciences **6**: 487–500. https://doi.org/10.5194/bg-6-487-2009

Duran, A., L. Collado-Vides, and D. E. Burkepile. 2016. Seasonal regulation of herbiviory and nutrient effects on macroalgal recruitment and succession in a Florida coral reef. PeerJ **4**: e2643. https://doi.org/10.7717/peerj.2643

Edson, J. B., Hinton, A. A., Prada, K. E, Hare, J.E., and Fairall, C. W. 1998 Direct covariance flux estimates from mobile platforms at sea. Journal of Atmospheric and Oceanic Technology **15**(2) 547–562. https://doi.org/10.1175/1520-0426(1998)015<0547:DCFEFM>2.0.CO;2

Edmunds, P. J., and P. S. Davies. 1986. An energy budget for *Porites porites* (Scleractinia). Mar. Biol. **92**: 339–347. https://doi.org/10.1007/BF00392674

Fischer, H. B., E. J. List, R. C. Y. Koh, J. Imberger, and N. H. Brooks. 1979. Mixing in inland and coastal waters, 1st ed. Acadmic Press.

Flügge, M., Paskyabi, M.B., Reuder, J., Edson, J.B., and Plueddemann, A.J.2016. Comparison of Direct Covariance Flux Measurements from an Offshore Tower and a Buoy. Journal of Atmospheric and Oceanic Technology **33**(5) 873–890. https://doi.org/10.1175/JTECH-D-15-0109.1

Gardner, T. A., I. M. Cote, J. A. Gill, A. Grant, and A. R. Watkinson. 2003. Long-term region-wide declines in Caribbean corals. Science **301**: 958–960. https://doi.org/10.1126/science.1086050

Gattuso, J. P., M. Frankignoulle, and R. Wollast. 1998. Carbon and carbonate metabolism in coastal aquatic ecosystems. Annu. Rev. Ecol. Syst. **29**: 405–434. https://doi.org/10.1146/annurev.ecolsys.29.1.405

Glud, R.N.2008. Oxygen dynamics of marine sediments. Mar. Biol. Res **4**: 243–289.

Gordon, M. S., and M. K. Hamilton. 1962. Primary productivity of an Hawaiian coral reef: A critique of flow Respirometry in turbulent waters. Ecology **43**: 473–480. https://doi.org/10.2307/1933375

Graham, N. A. J., and K. L. Nash. 2013. The importance of structural complexity in coral reef ecosystems. Coral Reefs **32**: 315–326. https://doi.org/10.1007/s00338-012-0984-y

Gueymard, C. 2005. Interdisciplinary applications of a versatile spectral solar irradiance model: A review. Energy **30**: 1551–1576. https://doi.org/10.1016/j.energy.2004.04.032

Haas, A. F., et al. 2011. Effects of coral reef benthic primary producers on dissolved organic carbon and microbial activity. PLoS One **6**: 12. https://doi.org/10.1371/journal.pone.0027973

Haas, A. F., and others. 2016. Global microbialization of coral reefs. Nat. Microbiol. **1**: 16042. https://doi.org/10.1038/NMICROBIOL.2016.42

Hartley, R., and A. Zisserman. 2003. Multiple view geometry in computer vision. Cambridge Univeristy Press.

Hatcher, B. G., and A. W. D. Larkum. 1983. An experimental analysis of factors controlling the standing crop of the epilithic algal community on a coral reef. J. Exp. Mar. Biol. Ecol. **69**: 61–84. https://doi.org/10.1016/0022-0981(83)90172-7

Hopkinson, B. M., A. C. King, D. P. Owen, M. Johnson-Roberson, M. H. Long, and S. Bhandarkar. 2020. Automated

classification of three-dimensional reconstructions of coral reefs using convolutional neural networks. PLoS One **15**: e0230671.https://doi.org/10.1371/journal.pone.0230671

Hughes, T. P. 1994. Catastrophes, phase shifts, and large-scale degradation of a Caribbean coral reef. Science **265**: 1547–1551. https://doi.org/10.1126/science.265.5178.1547

Hughes, T. P., and others. 2003. Climate change, human impacts, and the resilience of coral reefs. Science **301**: 929–933. https://doi.org/10.1126/science.1085046

Hughes, T. P., and others. 2007. Phase shifts, herbivory, and the resilience of coral reefs to climate change. Curr. Biol. **17**: 360–365. https://doi.org/10.1016/j.cub.2006.12.049

Joyce, K. E., and S. R. Phinn. 2002. Bi-directional reflectance of corals. Int. J. Remote Sens. **23**: 389–394. https://doi.org/10.1080/01431160110079420

Kirk, J. T. O. 2011. Light and photosynthesis in aquatic ecosystems, 3rd ed. Cambridge Univ. Press.

Kuhl, M., Glud, R.N., Ploug, H., and Ramsing, N.B. 1996. Microenvironmental control of photosynthesis and photosynthesis-coupled respiration in an epilithic cyanobacterial biofilm. Journal of Phycology **32**: 799–812.

Langdon, C. and others 2003. Effect of elevated CO2 on the community metabolism of an experimental coral reef. Global Biogeochemical Cycles 17

LeCun, Y., Y. Bengio, and G. Hinton. 2015. Deep learning. Nature **521**: 436–444. https://doi.org/10.1038/nature14539

Lirman, D., and P. Biber. 2000. Seasonal dynamics of macroalgal communities of the Northern Florida Reef tract. Bot. Marina **43**: 305–314. https://doi.org/10.1515/BOT.2000.033

Long, M. H., J. E. Rheuban, P. Berg, and J. C. Zieman. 2012. A comparison and correction of light intensity loggers to photosynthetically active radiation sensors. Limnol. Oceanogr.: Methods **10**: 416–424. https://doi.org/10.4319/lom.2012.10.416

Long, M. H., P. Berg, D. De Beer, and J. C. Zieman. 2013. In situ coral reef oxygen metabolism: An Eddy correlation study. PLoS One **8**. https://doi.org/10.1371/journal.pone.0058581

Long, M. H., P. Berg, K. J. Mcglathery, and J. C. Zieman. 2015. Sub-tropical seagrass ecosystem metabolism measured by eddy correlation. Mar. Ecol.-Prog. Ser. **529**: 75–90. https://doi.org/10.3354/meps11314

Long, M. H., and D. P. Nicholson. 2018. Surface gas exchange determined from an aquatic eddy covariance floating platform. Limnol. Oceanogr.: Methods **16**: 145–159. https://doi.org/10.1002/lom3.10233

Long, M. H., J. E. Rheuban, D. C. McCorkle, D. J. Burdige, and R. C. Zimmerman. 2019. Closing the oxygen mass balance in shallow coastal ecosystems. Limnol. Oceanogr. **64**: 2694–2708. https://doi.org/10.1002/lno.11248

Marsh, J. A. 1970. Primary productivity of reef-building calcareous red algae. Ecology **51**: 255–263.

McGillis, W. R., C. Langdon, B. Loose, K. K. Yates, and J. Corredor. 2011. Productivity of a coral reef using boundary layer and enclosure methods. Geophys. Res. Lett. **38**: 5. https://doi.org/10.1029/2010GL046179

Moran, P. J. 1986. The Acanthaster phenomenon. Oceanogr. Mar. Biol. **24**: 379–480.

Mueller, B., J. M. de Goeij, M. J. A. Vermeij, Y. Mulders, E. van der Ent, M. Ribes, and F. C. van Duyl. 2014. Natural diet of coral-excavating sponges consists mainly of dissolved organic carbon. PLoS One **9**: e90152. https://doi.org/10.1371/journal.pone.0090152

Muscatine, L., L. R. Mccloskey, and R. E. Marian. 1981. Estimating the daily contribution of carbon from zooxanthellae to coral animal respiration. Limnol. Oceanogr. **26**: 601–611. https://doi.org/10.4319/lo.1981.26.4.0601

Naumann, M. S., C. Jantzen, A. F. Haas, R. Iglesias-Prieto, and C. Wild. 2013. Benthic primary production budget of a Caribbean reef lagoon (Puerto Morelos, Mexico). PLoS One **8**: 8. https://doi.org/10.1371/journal.pone.0082923

Odum, H. T., and E. P. Odum. 1955. Trophic structure and productivity of a windward coral reef community on Eniwetok Atoll. Ecol. Monogr. **25**: 291–320. https://doi.org/10.2307/1943285

Ong, R. H., A. J. C. King, M. J. Caley, and B. J. Mullins. 2018. Prediction of solar irradiance using ray-tracing techniques for coral macro- and micro-habitats. Mar. Environ. Res. **141**: 75–87. https://doi.org/10.1016/j.marenvres.2018.08.004

Pawlik, J. R., and S. E. McMurray. 2020. The emerging ecological and biogeochemical importance of sponges on coral reefs. Ann. Rev. Mar. Sci. **12**: 315–337. https://doi.org/10.1146/annurev-marine-010419-010807

Rheuban, J. E., and P. Berg. 2013. The effects of spatial and temporal variability at the sediment surface on aquatic eddy correlation flux measurements. Limnol. Oceanogr.: Methods **11**: 351–359. https://doi.org/10.4319/lom.2013.11.351

Rheuban, J.E., Berg, P., and McGlathery, K.J. 2014. Ecosystem metabolism along a colonization gradient of eelgrass (Zostera marina) measured by eddy correlation. Limnology and Oceanography **59**: 1376–1387.

Richter, C., M. Wunsch, M. Rasheed, I. Kotter, and M. I. Badran. 2001. Endoscopic exploration of Red Sea coral reefs reveals dense populations of cavity-dwelling sponges. Nature **413**: 726–730. https://doi.org/10.1038/35099547

Ruzicka, R. R., and others. 2013. Temporal changes in benthic assemblages on Florida Keys reefs 11years after the 1997/1998 El Nino. Mar. Ecol.-Prog. Ser. **489**: 125–141. https://doi.org/10.3354/meps10427

Sawall, Y., and E. J. Hochberg. 2018. Diel versus time-integrated (daily) photosynthesis and irradiance relationships of coral reef organisms and communities. PLoS One **13**: 13. https://doi.org/10.1371/journal.pone.0208607

Smith, J. E., and others. 2006. Indirect effects of algae on coral: Algae-mediated, microbe-induced coral mortality. Ecol. Lett. **9**: 835–845. https://doi.org/10.1111/j.1461-0248.2006.00937.x

Takeshita, Y., and others. 2016. Assessment of net community production and calcification of a coral reef using a boundarylayer approach. J. Geophys. Res. Oceans **121**: 5655–5671. https://doi.org/10.1002/2016JC011886

Van Hoytema, N., V. N. Bednarz, U. Cardini, M. S. Naumann, F. A. Al-Horani, and C. Wild. 2016. The influence of seasonality on benthic primary production in a Red Sea coral reef. Mar. Biol. **163**: 14. https://doi.org/10.1007/s00227-015-2787-5

Wild, C., M. Huettel, A. Klueter, S. G. Kremb, M. Y. M. Rasheed, and B. B. Jorgensen. 2004. Coral mucus functions as an energy carrier and particle trap in the reef ecosystem. Nature **428**: 66–70. https://doi.org/10.1038/nature02344

Wild, C., W. Niggl, M. S. Naumann, and A. F. Haas. 2010. Organic matter release by Red Sea coral reef organisms-potential effects on microbial activity and in situ O-2 availability. Mar. Ecol.-Prog. Ser. **411**: 61–71. https://doi.org/10.3354/meps08653

Zepp, R. G., and others. 2008. Spatial and temporal variability of solar ultraviolet exposure of coral assemblages in the Florida Keys: Importance of colored dissolved organic matter. Limnol. Oceanogr. **53**: 1909–1922. https://doi.org/10.4319/lo.2008.53.5.1909

Acknowledgments

This work was supported by grants from the Alfred P. Sloan Foundation (BMH, BR2014-049) and the US National Science Foundation (MHL, OCE-1657727; BMH, DBI-2016741). Permits for the research were authorized by the Florida Keys National Marine Sanctuary (FKNMS-2016-042, FKNMS-2016-082, FKNMS-2017-35). We thank Jennie Rheuban for assistance with field work.

Conflict of Interest

None declared.

Submitted 13 April 2020
Revised 22 July 2020
Accepted 19 September 2020

Associate editor: Steeve Comeau